Astron. Astrophys. 338, 43–55 (1998)

ASTRONOMY AND ASTROPHYSICS

On the age of the nearby blue compact dwarf galaxy SBS 0335-052

P. Papaderos[1], **Y.I. Izotov**[2], **K.J. Fricke**[1], **T.X. Thuan**[3], **and N.G. Guseva**[2]

[1] Universitäts–Sternwarte, Geismarlandstraße 11, D-37083 Göttingen, Germany
[2] Main Astronomical Observatory of National Academy of Sciences of Ukraine, Goloseevo, 252650 Kiev-22, Ukraine
[3] Astronomy Department, University of Virginia, Charlottesville, VA 22903, USA

Received 27 April 1998 / Accepted 7 July 1998

Abstract. $UBVRI$ surface photometry and long-slit spectrophotometric observations are used to investigate the evolutionary status and put constraints on the age of the underlying stellar population of the eastern component of a nearby pair of dwarf galaxies, the blue compact dwarf galaxy SBS 0335–052E. We show that ionized gas emission extending out to distances $\gtrsim 1$ kpc from the central complex of super-star clusters (SSC) can significantly influence the observed colour distribution of the underlying component. After correction for the latter effect, we find that the intrinsic colours of the underlying component in SBS 0335–052E are consistent with those of a stellar population not older than 100 Myr, so that the BCD is truly a young galaxy.

Key words: galaxies: compact – galaxies: evolution – galaxies: individual: SBS 0335-052 – galaxies: ISM

1. Introduction

The search for young galaxies in the process of forming is one of the most challenging observational tasks in contemporary astrophysics and an essential requisite for understanding galaxy formation processes. The advent of HST and the Keck telescope has allowed the discovery and study of many distant galaxies at redshifts $z\geq$3 (Steidel et al. 1996; Giavalisco et al. 1996). However, it is still not clear whether genuine primeval galaxies have been discovered: the spectra of the high-redshift galaxies observed to-date all exhibit strong absorption lines of heavy elements, suggestive of an advanced evolutionary stage. Furthermore, their faintness and their small angular size make a detailed study of their properties very difficult.

An alternative approach is to study a subset of a class of nearby dwarf galaxies called Blue Compact Dwarf (BCD) galaxies. Even since their discovery (Sargent & Searle 1970), BCDs have been thought to be chemically unevolved systems presently undergoing one of their very first bursts of star formation (see Thuan 1991 for a review). This is mainly because BCDs are very metal-deficient, the metallicities of their ionized gas ranging between $Z_{\odot}$/50 and $Z_{\odot}$/3. Other evidence, such as the very high fractional neutral hydrogen gas content (Thuan & Martin 1981) and the lack of an evident underlying old stellar population on Palomar Sky Survey images, also point to the relative youth of some BCDs. However, subsequent multicolour investigations of BCDs (Loose & Thuan 1985; Kunth, Maurogordato & Vigroux 1988; Papaderos et al. 1996a; Telles & Terlevich 1997) have revealed that the majority of them ($\geq$ 95%) contain an extended and old low surface brightness (LSB) stellar population, and thus are not young galaxies but rather older gas-rich dwarf systems undergoing a transient starburst phase.

There is mounting evidence that extremely metal - deficient BCDs may not contain a significant old underlying stellar population and hence are prime candidates for being young galaxies. We focus our attention in this paper on one of the most metal-deficient BCDs known, the eastern component of a pair of dwarf galaxies, the BCD SBS 0335–052E. With a metallicity of only $Z_{\odot}$/40 (Izotov et al. 1990, Melnick, Heydari-Malayeri & Leisy 1992), this BCD is the second most metal-deficient BCD known after I Zw 18 ($Z_{\odot}$/50; Searle & Sargent 1972). Thuan, Izotov & Lipovetsky (1997) have argued that SBS 0335–052E is a truly young galaxy on the basis of the following evidence: 1) HST imaging shows the extended underlying LSB component of the BCD to have an irregular and filamentary structure, which suggests that a significant part of the emission comes from ionized gas. 2) Moreover, the underlying component shows, contrary to most BCDs investigated thus far, unusually blue colours, again indicative of gaseous emission.

There are other lines of evidence which point to a primordial nature of SBS 0335–052. A 21cm VLA map (Pustilnik et al. 1998) reveals that the BCD is embedded in an extremely large H I cloud with dimensions 67 kpc $\times$ 24 kpc and a total mass of some 2×10^9 $M_{\odot}$. The large size of this H I cloud is very unusual, as the H I envelope of most BCDs, including I Zw 18, is more of the order of a few kpc. The H I brightness distribution shows two peaks, one of which is coincident with SBS 0335–052E. Thuan & Izotov (1997) obtained HST UV spectrophotometry of the BCD and detected a broad damped Lyα absorption line. By fitting the Lyα absorption profile, they derived a neutral gas column density of N(H I) = 7×10^{21} cm^{-2} in the direction of SBS 0335–052E, comparable to the highest H I column densities derived for high-redshift damped Lyα galaxies.

Send offprint requests to: P. Papaderos

Analyzing the stellar metal absorption lines in the UV spectrum, and assuming that these lines arise in the H I envelope, Thuan & Izotov (1997) found the N(O)/N(H) ratio in the H I envelope of the BCD to be 37000 times smaller than the solar value. An even more consistent scenario put forward by the same authors considers the metal absorption lines not to arise in the H I but rather in the H II gas. In this case, the H I envelope around SBS 0335–052E would be truly primordial, unpolluted by any heavy element. Either scenario would support strongly the hypothesis of SBS 0335–052 being very young. The second H I peak, located at a distance of 22 kpc to the west, also possesses an optical counterpart, SBS 0335–052W. Pustilnik et al. (1997) have shown it to be a fainter ($V \sim 19$ mag) dwarf galaxy. Optical spectrophotometry by Lipovetsky et al. (1998) shows it to have lower excitation but to be as metal-deficient as its eastern companion.

Although the above observations strongly point to the youth of SBS 0335–052, there was also evidence that the underlying extended low surface brightness component of this BCD is not purely gaseous in nature, but contains also stars. Izotov et al. (1997b) found from detailed spectroscopic studies that the observed equivalent width of the Hβ emission in the underlying component to be $\sim$3 times lower than the value expected in the case of pure gaseous emission. In other words, $\sim$2/3 of the underlying emission in the BCD originates from a stellar background population. Thus, to put constraints on the age of the BCD, we have to study the underlying stellar population, which we do here with deep $UBVRI$ surface photometry. A major problem in interpreting the photometric data is the widespread and spatially varying contamination of the underlying light by gaseous emission from supergiant H II regions surrounding the central ionizing super-star clusters (SSC). The nebular emission lines and the gaseous continuum influence strongly the observed colours and should be subtracted out before the photometric data can be analyzed in terms of stellar populations (Izotov et al. 1997b). We discuss the photometric data in Sect. 2. New U and B observations are presented. Spectroscopic observations are discussed in Sect. 3. The surface brightness profiles are described in Sect. 4. In Sect. 5 we determine the age of SBS 0335–052 by computing synthetic colours and model spectral energy distributions and comparing with the data. A distance of 54.3 Mpc is adopted throughout for SBS 0335–052. At this distance, one arcsec corresponds to 263 pc.

2. Photometric observations

The new photometric data discussed here consist of two sets: one obtained at Calar Alto, Spain (September 19, 1996) and the other at La Silla (November 6, 1996). The Calar Alto data were obtained with the CAFOS focal reducer attached to the 2.2m telescope. The CCD-detector was a 2090 $\times$ 2090 pixel SITe with an instrumental scale of 0.″53 pixel^{-1}, operating at a gain of 2.3 $\mathrm{e}^-/\mathrm{ADU}$. The field of view was $\sim 17'$ in diameter. SBS 0335–052 was observed under non-photometric conditions for 20 min in Johnson U and 5 min in Johnson B with a seeing of FWHM = 1.″40 $\pm$ 0.″06 and 1.″17 $\pm$ 0.″05 in U and B, respectively. W. Pietsch (MPE-Garching) and K. Bischoff (Göttingen) kindly obtained the second set of U and B exposures for us. These observations were done under photometric conditions, which allowed us to calibrate the first set. The instrumental set-up consisted of the focal-reducer EFOSC and a 2048$\times$2048 Loral/Lesser-chip with a scale of 0.″262 pixel^{-1}, operating in the high gain mode (1.4 $\mathrm{e}^-/\mathrm{ADU}$). The FWHM of point sources, was determined to 1.″57 $\pm$ 0.″08 in U and 1.″45 $\pm$ 0.″06 in B. Photometric calibration was provided by observations of the standard star PG 0231+051 field (Landolt 1992). The MIDAS software package was used to apply the standard reduction procedures (cosmic-ray removal, dark, bias, and flat-field corrections) to the CCD frames. The background-subtracted images from both runs were then coadded. Table 1 lists the integrated U and B photometry for both SBS 0335–052E and SBS 0335–052W (Fig. 1). We have also included photometric data in other bands from the literature. The accuracy of the positions listed in Table 1 is estimated to be $\sim 1''$.

Table 1. Integrated photometric properties of SBS 0335–052

Parameter	SBS 0335–052E	SBS 0335–052W	Ref.
RA(2000)	$03^{\mathrm{h}}37^{\mathrm{m}}44^{\mathrm{s}}.03$	$03^{\mathrm{h}}37^{\mathrm{m}}38^{\mathrm{s}}.40$	1
DEC(2000)	$-05^\circ02'38''.8$	$-05^\circ02'36''.4$	1
U (mag)	16.24 ± 0.04	18.74 ± 0.08	1
B (mag)	16.96 ± 0.02	19.29 ± 0.07	1
V (mag)	16.65 ± 0.01	—	2
R (mag)	16.57 ± 0.01	19.03 ± 0.05	3
I (mag)	16.88 ± 0.01	19.08 ± 0.05	2,3
$U-B$ (mag)	-0.72 ± 0.05	-0.54 ± 0.10	
$B-V$ (mag)	0.31 ± 0.03	—	
$V-I$ (mag)	-0.23 ± 0.02	—	
$R-I$ (mag)	-0.35 ± 0.02	-0.05 ± 0.07	

References: 1 – this paper; 2 – Thuan et al. (1997); 3 – Lipovetsky et al. (1998).

3. Spectroscopic observations

Spectrophotometric observations of SBS 0335–052E were acquired with the Multiple Mirror Telescope (MMT) on the night of 1995 December 20. A signal-to-noise ratio of $\sim$ 30 was obtained in the continuum of the bright central part. Observations were made in the blue channel of the MMT spectrograph using a highly optimized Loral 3072$\times$1024 CCD detector. A 1″$\times$180″ slit was used along with a 500 groove mm^{-1} grating in first order and an L-38 second-order blocking filter. This yields a spatial resolution along the slit of 0.″3 pixel^{-1}, a scale perpendicular to the slit of 1.9 Å pixel^{-1}, a spectral range 3600–7500Å, and a spectral resolution of $\sim$7Å FWHM. For these observations, CCD rows were binned by a factor of 2, yielding a final spatial sampling of 0.″6 pixel^{-1}. The observations have sufficient spectral resolution to separate [O III] λ4363 from the nearby Hγ line and thus permit a reliable determination of the electron temperature in the H II region. The total exposure time of 60 minutes was broken up into three subexposures, 20 minutes each, to al-

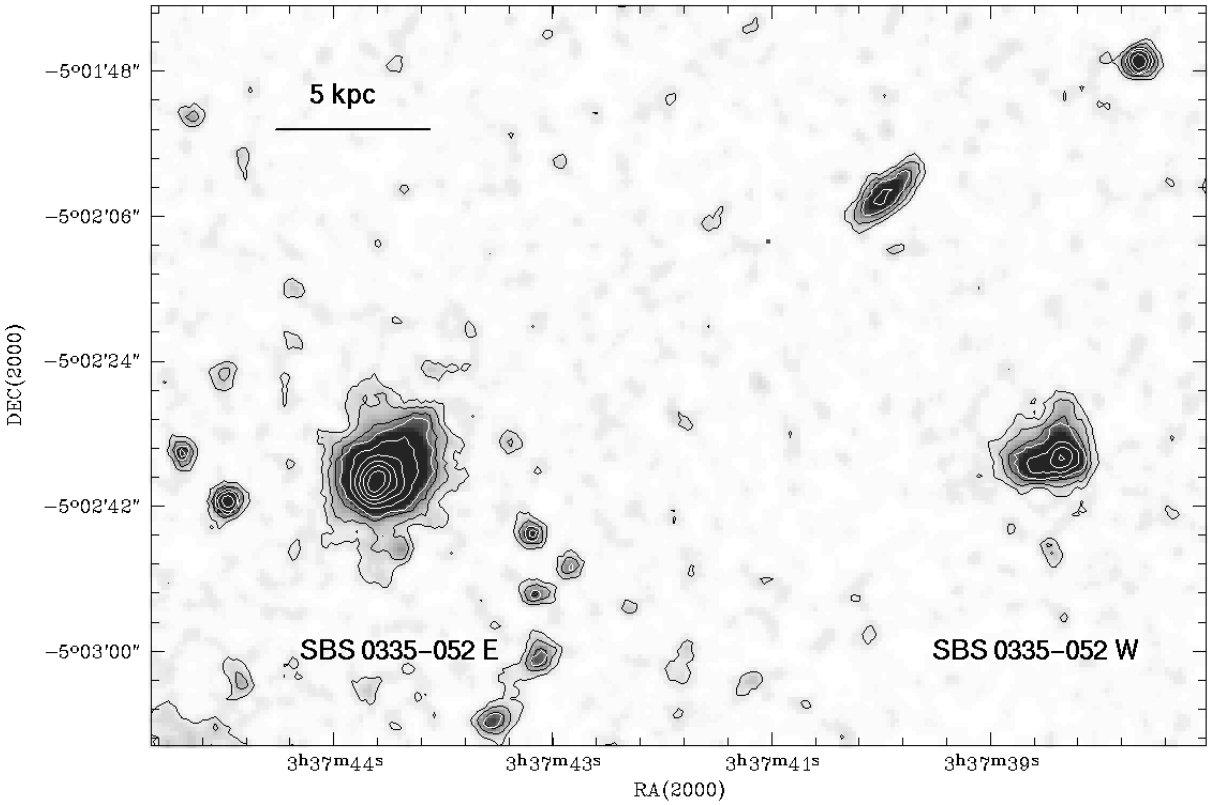

Fig. 1. B band exposure of SBS 0335–052. The two members of the system are separated by $1\farcm41$ (22.3 kpc). The chain of point-like sources at $\sim 28''$ southwest of SBS 0335–052E is seen from HST WFPC2 images to represent background galaxies. Contours go from 20 to 25 B mag arcsec^{-2} and from 25.5 to 27.5 B mag arcsec^{-2} in steps of 1 mag. As shown in Thuan et al. (1997), the slight extension of SBS 0335–052E to the northwest is caused by both an intrinsic asymmetry of the underlying LSB component and the presence of a large starburst-driven supershell. Note that the more compact SBS 0335–052W contains at least two components . The fainter one (fainter by ~ 1.4 B mag in its mean surface brightness) is located about $3\farcs5$ to the east of the central brighter component.

low for more effective cosmic-ray removal. All exposures were taken at small airmasses ($\leq$1.27), so no correction was made for atmospheric dispersion. The seeing during the observations was $1''$ FWHM. The slit was oriented in a position angle of –30° (determined from high resolution HST images) to permit observations of all stellar clusters and low-intensity extended emission. The spectrophotometric standard star PG 0216+032 was observed for flux calibration. Spectra of He-Ne-Ar comparison lamps were obtained before and after each observation to provide wavelength calibration.

Data reduction of the spectral observations was carried out at the NOAO headquarters in Tucson using the IRAF software package. This included bias subtraction, cosmic-ray removal and flat-field correction using exposures of a quartz incandescent lamp. After wavelength mapping, night-sky background subtraction, and correcting for atmospheric extinction, each frame was calibrated to absolute fluxes.

One-dimensional spectra were extracted by summing, without weighting, different numbers of rows along the slit depending on the exact region of interest. The emission line intensities were measured by fitting Gaussians to the profiles in each region along the slit with size $0\farcs6\times1''$ giving in total 21 one-dimensional spectra. To derive both the extinction coefficient $C(\mathrm{H}\beta)$ and the absorption equivalent width for the hydrogen lines, an iterative procedure described by Izotov et al. (1994, 1997a) has been employed. Elemental abundances were derived following the procedure by Izotov et al. (1994, 1997a) as well.

The auroral emission line [O III] λ4363 was detected in each of the 21 one-dimensional spectra covering a total angular size of $13''$ ($\sim$ 3.4 kpc). Therefore, the electron temperature T_e(O III) was determined from the [O III] λ4363/ $\lambda\lambda$(4959 + 5007) ratio and the electron number density N_e(S II) from the [S II] λ6717/λ6731 ratio. More details of the data reduction are presented by Izotov et al. (1997b) where it was shown that within the supergiant H II region of $\lesssim$ 4 kpc in diameter the electron temperature T_e is nearly constant at $\sim$ 20000 K and the oxygen abundance remains also constant at $\sim$1/40 solar.

3.1. Synthetic spectral energy distribution

The stellar emission in SBS 0335–052 is strongly contaminated by emission of ionized gas from supergiant H II regions in both the eastern and western components (Izotov et al. 1997b; Lipovetsky et al. 1998). Therefore, to study the stellar composition in SBS 0335–052 using broad-band photometric data it

is necessary to construct a synthetic spectral energy distribution (SED) which includes both stellar and ionized gaseous emission. For analysis of the stellar content of the young ionizing clusters in SBS 0335–052E we have chosen the SEDs calculated by Schaerer & Vacca (1998) for various metallicities and ages in the range Z = 0.001–0.02 and t = 0.1–10 Myr, respectively. The age of the extended underlying stellar population in SBS 0335–052E has been estimated to be greater than 10 Myr (Izotov et al. 1997b; Thuan et al. 1997). Therefore, we have calculated a grid of SEDs for stellar populations with ages ranging between 10 Myr and 20 Gyr and heavy element abundances $Z/Z_{\odot}$ varying between 10^{-5} and 10 using isochrones based on stellar parameters from Bertelli et al. (1994) and the compilation of stellar atmosphere models from Lejeune et al. (1997). Initial Mass Functions (IMFs) with slopes –2, –2.35 (Salpeter), –3 and a lower mass limit of $0.6M_{\odot}$ were adopted. We have chosen not to calculate the contribution of ionized gas emission from the model value for the Lyman continuum luminosity and subtract it from the total emission to derive the stellar populations. Instead, we add different calculated stellar spectral energy distributions to the observed gaseous spectral energy distribution to match the observed total emission. The derived stellar population would correspond to the one which gives the best match. The contribution of gaseous emission was scaled to the stellar emission by the ratio of the observed equivalent width of the Hβ emission line to the equivalent width of Hβ expected for pure gaseous emission. The gaseous emission at any location in the BCD is mainly due to the ionizing radiation of the brightest SSCs discovered by Thuan et al. (1997) at the center of the galaxy. To calculate the gaseous continuum spectral energy distribution at each point along the slit, the observed Hβ flux and the electron temperature are derived from the spectrum at that point. The contribution of bound-free, free-free, two-photon continuum emission are then calculated for the spectral range from 0 to 5 μm (Aller 1984; Ferland 1980). We then superpose on the gaseous continuum SED the contribution by the emission lines, the intensities of which were derived from the observed spectra in the spectral range $\lambda\lambda$3700 – 7500Å. Outside this range the emission line intensities (mainly hydrogen lines) are calculated from the intensity of Hβ corrected for intrinsic extinction.

4. Results

Fig. 2 shows the surface brightness profiles (SBPs) of SBS 0335–052E in the U (filled circles) and B (open circles) as derived from the combined broad band images obtained at Calar Alto and La Silla. Error bars correspond to 2σ uncertainties estimated as described in Papaderos et al. (1996a) and take into account the detector gain and photon statistics for each frame. Straight lines represent exponential fits to the intensity distribution for radii $> 4''$, weighted by the photometric uncertainties of each SBP. The residual light distribution in excess of the exponential fitting law is shown by the solid curves. Assuming that the LSB component of SBS 0335–052E can be properly described all the way to $R^* = 0$ by an exponential law, the excess light above the exponential fit provides a measure of the size and luminosity of the starburst component. The radial extent of the BCD at 25 mag arcsec^{-2} as deduced from the linear fits is E^U_{25}=6.″97 (1.84 kpc) and E^B_{25}=5.″8 (1.53 kpc) in U and B, respectively. The linear fits to the outer exponential component of SBS 0335–052E yield central surface brightnesses of $\mu^U_{\rm E,0} = 20.66 \pm 0.08$ mag arcsec^{-2}and $\mu^B_{\rm E,0} = 21.38 \pm 0.05$ mag arcsec^{-2} (Table 2). Note that the central surface brightness of the LSB component of SBS 0335–052E compares well with the mean value of 21.3±0.15 mag arcsec^{-2} obtained by Papaderos et al. (1996b) for a sample of more evolved BCDs. However, the light of the diffuse LSB component in the latter systems comes from stellar populations with ages greater than a few Gyrs, which are thus, as we shall see, much older than the ones in SBS 0335–052E.

The corresponding exponential scale lengths are $\alpha_U = 1.''74 \pm 0.''04$ (459±12 pc) and $\alpha_B = 1.''74 \pm 0.''03$ (458±8 pc). These are again compatible to those determined for the LSB component of other BCDs (Papaderos et al. 1996b, Telles & Terlevich 1997). They are also similar to $\alpha_V = \alpha_I = 0.42$ kpc obtained for the BCD Mrk 996 which possesses an unusually dense star-forming region (Thuan, Izotov & Lipovetsky 1996). Extrapolation of the exponential slope deduced for the LSB component of SBS 0335–052E to $R^* = \infty$ yields total apparent luminosities of $m^U_{\rm LSB}\infty = 17.45$ mag and $m^B_{\rm LSB}\infty = 18.18$ mag (Table 2), thus a mean $(U-B)$ colour index of –0.73 mag. Furthermore, the fact that the scale lengths of the LSB component in SBS 0335–052E in either bands agree to better than 1%, implies a zero colour gradient for the LSB component. This is also the case for the residual starburst light above the exponential law (Fig. 2). The constancy of the radially averaged $(U-B)$ colour index of SBS 0335–052E over a linear range between and $2''$ and $10''$ at $\sim -0.75 \pm 0.1$ mag is demonstrated in Fig. 4. Correcting for galactic extinction will make the $(U-B)$ colour bluer by ~ -0.06 mag.

Fig. 3 displays the V and I surface brightness profiles of SBS 0335–052E as derived from HST WFPC2 data, after removal of the luminosity contribution of the northern gaseous loop and of compact sources at distances greater than $3''$ from the brightest SSC (No. 1 in the nomenclature of Thuan et al. 1997; cf. Fig. 9). Thus, Fig. 3 shows the radial intensity distribution of the diffuse LSB component in SBS 0335–052E. The SBPs shown here differ slightly from the ones given in Thuan et al. (1997) for radii greater than $3''$ because those authors did not remove the luminosity of the compact sources. Both surface photometry approaches lead, however, to the same conclusion, that the $(V-I)$ colour index of the LSB component in SBS 0335–052E is nearly constant. By direct subtraction of the I profile from the V profile (Fig. 5) we derive for $R^* > 3''$ a mean colour index of -0.06 ± 0.02 mag for the LSB component, close to the value of $(V-I) \sim 0.0$ mag obtained by Thuan et al. (1997). Note, however, that for smaller radii a direct profile subtraction does not correctly reproduce the colour distribution (cf. Fig. 9a). This effect, discussed in detail in Papaderos et al. (1996a), is due to the fact that the bluest regions within a galaxy do not necessarily coincide with the most luminous ones.

Table 2. Structural properties of SBS 0335–052 in different bands

Name	Band	$\mu_{\rm E,0}$ mag arcsec^{-2} (1)	α pc (2)	P_{25} kpc (3)	$m_{P_{25}}$ mag (4)	E_{25} kpc (5)	$m_{E_{25}}$ mag (6)	$m_{\rm LSB\,\infty}$ mag (7)	m_∞ mag (8)	Notes
SBS 0335–052E	U	20.66 ± 0.08	459 ± 12	1.00	16.68	1.84	17.56	17.45	16.25 ± 0.04	a
SBS 0335–052E	B	21.38 ± 0.05	458 ± 8	0.90	17.44	1.53	18.35	18.18	17.00 ± 0.02	a
SBS 0335–052E	V	20.71 ± 0.26	376 ± 30	0.55	17.1	1.48	18.06	17.95	16.69 ± 0.04	b
SBS 0335–052E	R	21.61 ± 0.1	610 ± 15	1.01	16.92	1.90	18.00	17.79	16.54	c
SBS 0335–052E	I	20.96 ± 0.35	396 ± 43	0.61	17.22	1.47	18.21	18.08	16.82 ± 0.05	b
SBS 0335–052W	U	22.27 ± 0.34	402 ± 40	0.76	19.74	1.01	19.72	19.35	18.78 ± 0.08	a
SBS 0335–052W	B	22.33 ± 0.22	387 ± 20	0.36	21.74	0.95	19.88	19.5	19.37 ± 0.06	a

[a] this paper; [b] HST archival data. The structural properties of the LSB component listed in Cols. 5–8 are obtained after subtraction of point sources; [c] data from Lipovetsky et al. (1998).

(1) Central surface brightness of the LSB component obtained from a linear fit to the outer parts of each SBP, weighted by its photometric uncertainties.
(2) Exponential scale length of the LSB component. A distance of 54.3 Mpc to SBS 0335–052 is assumed.
(3) Linear extent of the luminous component in excess of the LSB component at a surface brightness level of 25 mag arcsec^{-2}.
(4) Apparent magnitude of the starburst component within P_{25}.
(5) Linear extent of the LSB component determined from the fit.
(6) Apparent magnitude of the LSB component within E_{25}.
(7) Total apparent magnitude of the LSB component estimated by extrapolation of the exponential fitting law to $R^* = \infty$.
(8) Total apparent magnitude of the target from extrapolation of the SBPs (cf. Table 1).

Fig. 6 displays the surface brightness profiles of SBS 0335–052W in U and B decomposed in the same fashion as those of SBS 0335–052E (Fig. 2). Similar to SBS 0335–052E, for radii greater than $\sim 4''$, the LSB component of SBS 0335–052W exhibits a nearly exponential intensity decrease. Linear fits to both SBPs in the latter range along with the residual intensity distribution in excess of the exponential LSB component, are displayed with thin and thick lines for U and B, respectively. At a surface brightness of 25 mag arcsec^{-2} the linear fits (Fig. 6) imply sizes of $E_{25}^U = 3\farcs85$ (1.01 kpc) and $E_{25}^B = 3\farcs6$ (0.95 kpc). The fits yield central surface brightnesses $\mu_{\rm E,0}^U = 22.3 \pm 0.3$ mag arcsec^{-2}and $\mu_{\rm E,0}^B = 22.3 \pm 0.2$ mag arcsec^{-2}. The corresponding angular exponential scale lengths are $\alpha_U = 1\farcs53 \pm 0\farcs15$ and $\alpha_B = 1\farcs47 \pm 0\farcs07$. Adopting the same distance for SBS 0335–052W as for SBS 0335–052E, the latter values translate to linear scale lengths of 402 ± 40 pc and 387 ± 20 pc, respectively. Thus, the LSB component of SBS 0335–052W is, in terms of its exponential scale length, slightly more compact than the LSB component of its eastern counterpart. Hence, its smaller total B luminosity as compared to that of the LSB component of SBS 0335–052E (19.5 mag vs. 18.18 mag) is mainly due to its fainter B central surface brightness (22.33 mag arcsec^{-2} vs. 21.38 mag arcsec^{-2}; Table 2). Despite the large photometric uncertainties inherent to the faintness and compact angular extent of SBS 0335–052W , it may be seen that the $(U-B)$ colour profile increases gradually with increasing galactocentric distance, with a possible flattening at $(U-B) = -0.2 \pm 0.15$ mag for its LSB component.

5. Discussion

5.1. Population synthesis models and the colours of young star-forming regions

Thuan et al. (1997) using HST WFPC2 V and I imaging have discovered 6 young compact SSCs in the southeastern part of SBS 0335–052E. These clusters are aligned along the major axis of the central supergiant H II region and show a steady increase of their extinction-corrected colours $(V-I)_0$ from –0.61 mag for the brightest SE cluster No.1 to +0.31 mag for the faintest NW cluster No.6, at a distance $\sim 2''$ ($\sim$ 500 pc) from SSC 1. Thuan et al. (1997) noted that the $(V-I)_0$ colour of SSC 1 is too blue to be explained by pure stellar emission, since the hottest O main-sequence star produces a $(V-I)_0$ colour ~ -0.33 mag. Therefore, for regions being bluer than the latter cutoff the observed colour can be plausibly explained by a contamination by gaseous emission, especially in the V band, where several strong emission lines are present.

In Table 3 we show the time evolution of various colours calculated first for the stellar emission alone and second for the sum of stellar and gaseous emission in the central part of SBS 0335–052E, using the stellar SEDs of clusters from Schaerer & Vacca (1998), with age in the range 2 – 10 Myr and a metallicity of Z=1/20 $Z_\odot$. The model SEDs were redshifted (z=0.0136) to compare directly with the observed SED. The ionized gas emission, corrected for intrinsic extinction with the extinction coefficient C(Hβ) = 0.24 derived from the observed hydrogen Balmer emission line ratios, was then added to the model stellar emission. For the sake of completeness we have also included $(V-K)$ colours in Table 3. Inspection of Table 3 demonstrates that, while the $(U-B)$ colour is relatively insensitive to the

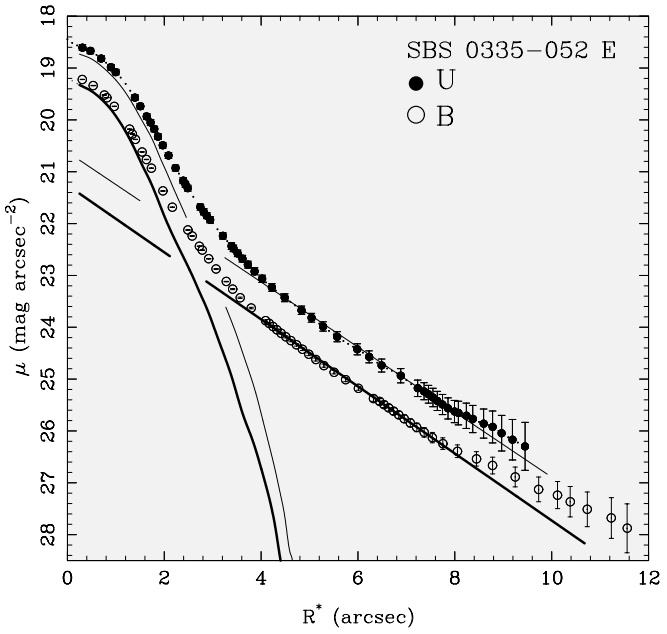

Fig. 2. Linear representation of the surface brightness profiles (SBPs) of SBS 0335–052E in U (filled circles) and B (open circles) calculated from the coadded frames (cf. Sect. 2). Error bars correspond to 2σ uncertainties. Linear fits for radii $> 4''$ weighted by the photometric uncertainties of each SBP are shown by thin and thick solid lines for U and B, respectively. The curves show the light distribution of the starburst component as obtained from subtraction of the exponential fit from each SBP. Note, that aside from a nearly constant vertical offset the SBPs of SBS 0335–052E in U and B are very similar, implying a constant colour for both, the starburst and the LSB component.

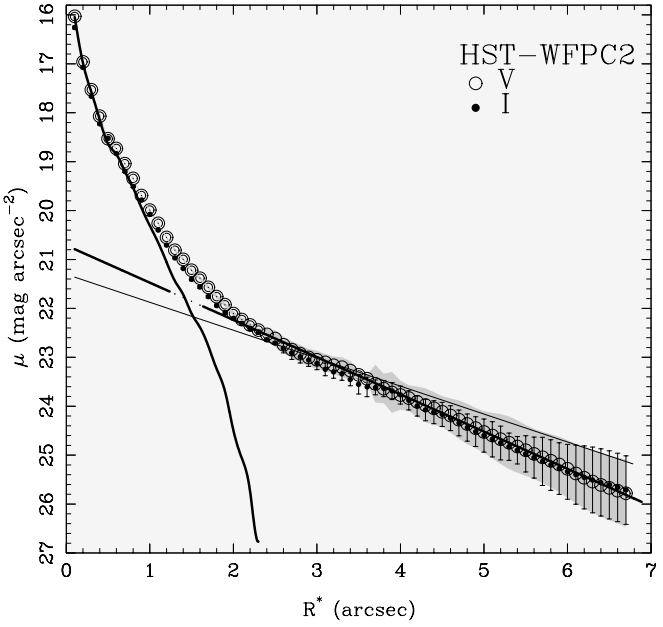

Fig. 3. Surface brightness profiles of SBS 0335–052E in V (open circles) and I (filled circles) derived from HST WFPC2 images, after removal of emission from the northern loop and compact sources at distance greater than $3''$ from super-star cluster 1 (cf. Fig. 9). Note that for radii $\gtrsim 3''$ both profiles are indistinguishable with a mean $(V-I)$ colour of -0.06 ± 0.02 mag. This value is close to the upper colour limit of ≈ 0.0 mag derived in Thuan et al. (1997). As in Fig. 2 the V luminosity of the central starburst component (thick curve) is described by the excess above the exponential intensity distribution, obtained by a linear fit for radii $> 3\farcs4$. The thin solid line shows the linear fit to the LSB component of the galaxy when the emission of the resolved compact sources is not subtracted.

presence of gaseous emission, contamination by ionized gas causes a pronounced change in the other colours.

In Fig. 7 the spectrum of the brightest part of SBS 0335–052E (thin line) is shown along with a synthetic gaseous + stellar continuum computed for a SSC having undergone an instantaneous burst of age 3 Myr. The large difference between the observed spectrum and the model continuum spectral energy distribution in the wavelength range $\lambda\lambda$3600–3900 is caused by the combination of two effects. First, there is the presence of Balmer hydrogen emission lines in the observed spectrum which are not taken into account in the model spectrum. The difference between observed and model spectra is significantly reduced when Balmer hydrogen emission lines are included in the model spectrum. Second, the model spectrum systematically overestimates the Balmer absorption lines. In Fig. 8 the contributions of gaseous and stellar emission to the combined spectrum are shown separately. It is evident that the contribution of the ionized gas emission to the total SED is significant in star-forming regions. This contribution is dependent on the equivalent width of Hβ and the observed intensities of emission lines relative to Hβ. Table 3 shows that the observed colours of the bluest clusters in SBS 0335–052E (cf. Table 4) cannot be reconciled with a pure stellar origin. By contrast, for all clusters except SSC No. 1 a combined gaseous + stellar synthetic SED produces $(V-I)$ colours in good agreement with the observations. The failure of the synthetic model to reproduce the $(V-I)_0$ of SSC No. 1 (the latter is too blue by $\sim$0.2 mag) could be the result of underestimating the local luminosity fraction contributed by ionized gas. This would happen if there is a steep gradient in the gas emissivity and/or a local metallicity increase. In the latter case, local polution of gas by heavy elements may lead to enhanced [O III]λ5007 emission compared to the average background value determined from ground-based spectroscopy for a substantially larger area. This line is a major contributor of gaseous emission in the V-band.

In principle, the colours of the reddest clusters in SBS 0335–052E within $< 2''$ from cluster No. 1 (SSCs 5 and 6) can be explained by stellar emission alone. However, spectral observations (Izotov et al. 1997b) show that the light of these clusters is strongly contaminated by gaseous emission as well, so that the intrinsic colours of the stellar emission are redder than those observed. These redder intrinsic colours relative to cluster 1 are due to two effects: the larger age of clusters 5 and 6, and the presence of dust which is clearly seen in the HST images obtained by Thuan et al. (1997). In Figs. 9a&b are shown V and I HST images of SBS 0335–052E processed with a hierarchical binning method (Papaderos et al. 1998). This method based on a local estimation and iterative subtraction of features greater

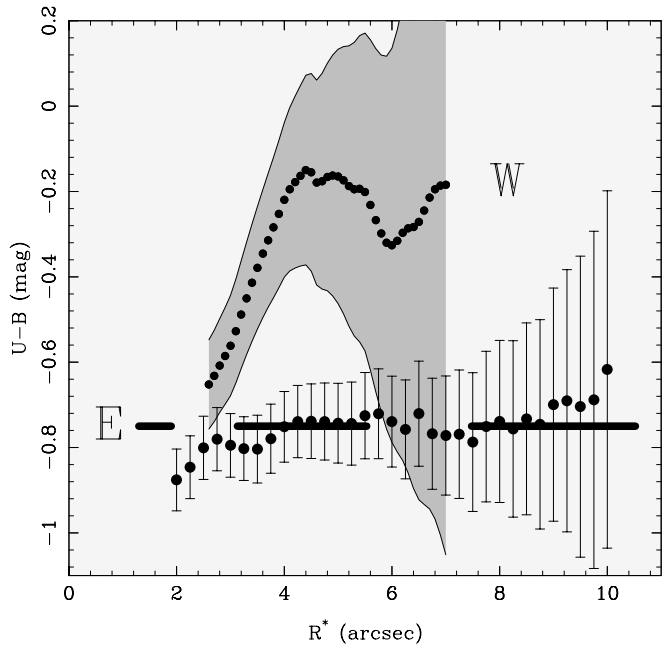

Fig. 4. $(U-B)$ profiles of SBS 0335–052E and SBS 0335–052W as derived from subtraction of the B-band profile from the U-band profile. The B-band profile was convolved to the lower resolution of the U-band profile. The thick line indicates the mean $(U-B)$ colour index of –0.75±0.1 mag deduced for the LSB component. This value is an upper limit since the colour is not corrected for galactic extinction. Taking into account photometric uncertainties, there is no $(U-B)$ colour gradient in SBS 0335–052E. As for its compact counterpart SBS 0335–052W, the colour profile shows a gradient for radii $\lesssim 4''$and levels off to a constant $(U-B)$ colour of -0.2 ± 0.15 mag in the outer part of the galaxy.

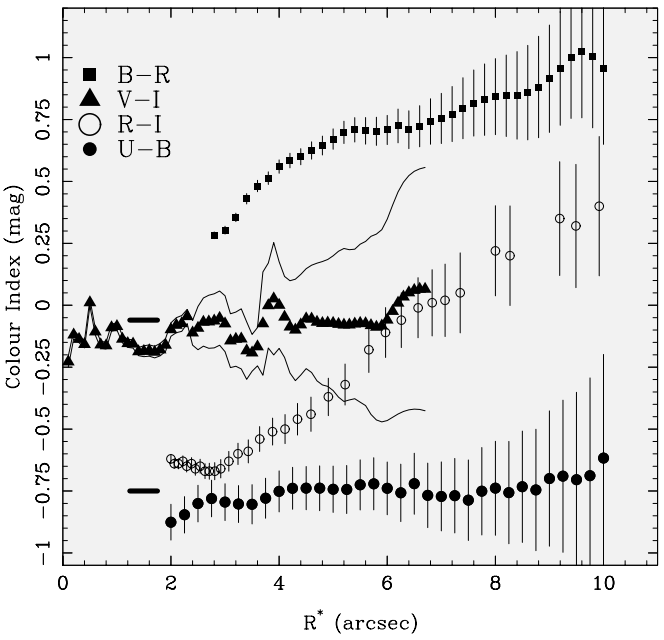

Fig. 5. $(U-B)$ and $(V-I)$ radial colour profiles of SBS 0335–052E. The mean colours $(U-B)$=–0.75±0.1 mag and $(V-I)$=–0.06±0.02 mag for the LSB component are shown by the thick lines. We have also shown the $(B-R)$ and $(R-I)$ profiles from the surface photometry by Lipovetsky et al. (1998).

Table 3. Synthetic colours for the central part of SBS 0335–052E

log t	$U-B$	$B-V$	$V-I$	$R-I$	$V-K$
			a) Stellar emission		
6.3	–1.14	–0.21	–0.14	–0.12	–0.70
6.6	–0.71	–0.05	0.04	–0.04	–0.24
6.7	–0.67	0.03	0.19	0.04	0.10
7.0	–0.86	–0.10	0.02	–0.06	–0.16
			b) Stellar and gaseous emission		
6.3	–0.96	0.20	–0.44	–0.43	0.12
6.6	–0.64	0.29	–0.32	–0.35	0.23
6.7	–0.61	0.34	–0.21	–0.28	0.34
7.0	–0.75	0.26	–0.33	–0.37	0.25
obs	...	...	–0.6÷0.2	...	...

than a given angular size is well suited for detecting faint structures embedded in a diffuse background. The gray map in the processed V image of SBS 0335–052E (Fig. 9a) shows the presence of several extra compact sources, in addition to the 6 SSCs already discussed by Thuan et al. (1997), most of them being aligned to the direction of the supershell. Note that in addition to the outer supershell discussed by Thuan et al. (1997) and located roughly 1.4 kpc from SSC 1, a second fainter loop is visible at roughly 1 kpc from SSC 1. The superimposed contours correspond to $(V-I)_0$ isochromes from –0.7 to –0.3 mag in steps 0.1 mag. From Fig. 9a is evident that the bluest $(-0.8 \lesssim (V-I)_0 < -0.6)$ regions in SBS 0335–052E designated A and B are not coincident with the brightest SSCs, but rather displaced by some ~ 100 pc.

This offset can be understood by the fact that the $(V-I)$ colour for stellar emission in SBS 0335–052E is redder than that for gaseous emission. While the $(V-I)_0$ index for the youngest stellar composite with age 2 Myr is –0.14 mag (Table 3), the $(V-I)$ colour produced by ionized gas with the emission line intensities observed in SBS 0335–052E, is ∼–0.75 mag. Therefore, the bluest regions in SBS 0335–052E are not necessarily associated with the SSCs. Rather they are those where, in the absence of any appreciable stellar background, ionized gas dominates the light. The main body of the supershell exhibits $(V-I)_0$ colours ranging between –0.3 and –0.4 mag. Its extremes are bluer, the western tip (region C) having a colour of $\lesssim -0.73$ mag, and the eastern tip (region D) a colour of $\lesssim -0.63$ mag. The presence of enhanced V emission on scales ~ 3 times the exponential scale length of the LSB component in SBS 0335–052E corroborates the spectroscopic evidence for an extended and spatially varying emission from an ionized gas component (Izotov et al. 1997b).

Thuan et al. (1997) discovered a systematic reddening of the clusters away from the brightest one (SSC 1). Because the new processing of the HST images allows to go fainter, we can extend their $(V-I)_0$ vs. distance analysis to lower luminosities and larger distances from SSC 1. The additional faint sources

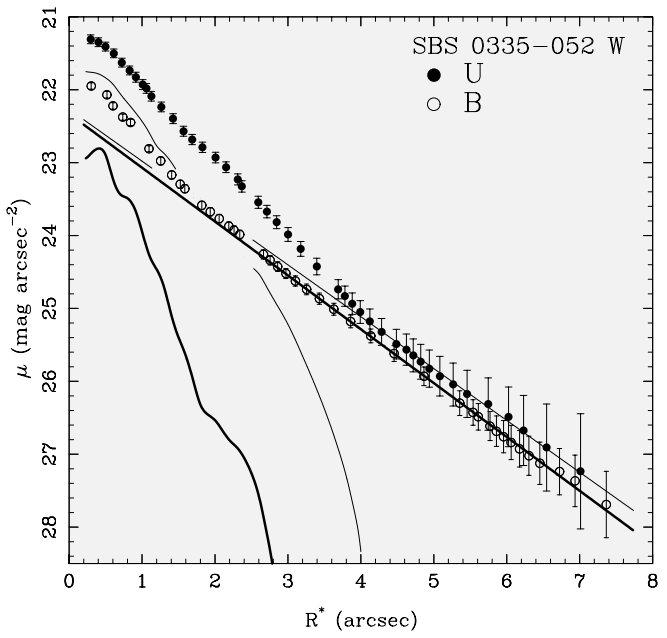

Fig. 6. Linear representations of the U and B surface brightness profiles of SBS 0335–052W. The solid lines have the same meaning as in Fig. 2. Note that, in contrast to SBS 0335–052E, the intensity distribution of the starburst component in SBS 0335–052W appears more extended in U than in B.

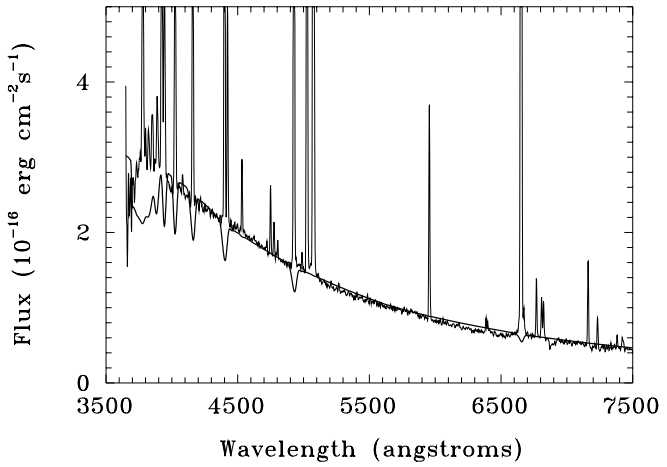

Fig. 7. Spectrum of the central part of SBS 0335–052E (thin line) superposed on a synthetic continuum including the gaseous and stellar emission with age 3 Myr (thick line). The large difference between the observed spectrum and model continuum distribution at wavelengths $\lambda\lambda$3600–3900 is caused by a combination of the presence of Balmer hydrogen emission lines in the observed spectrum and an overestimate of the Balmer absorption line strengths in the model.

are shown in Fig. 9b and their positions along with photometric data are listed in Table 4. The nomenclature for SSCs 1 to 6 is the same as in Thuan et al. (1997). Most of the new clusters also lying roughly along the major axis of the BCD have absolute luminosities $\gtrsim -10$ mag, thus they do not qualify as SSCs (cf. O'Connell et al. 1994 and references therein).

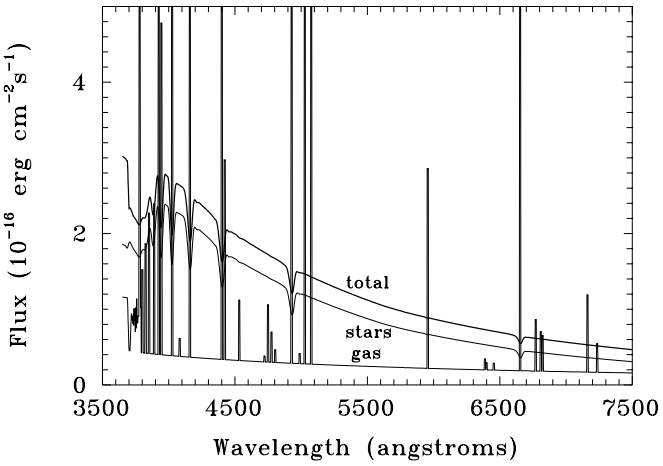

Fig. 8. Spectral energy distributions of the gaseous and stellar components of the central part of SBS 0335–052E (thin lines). The total composite continuum energy distribution is shown by the thick line.

In Fig. 10 we plot the projected angular distance from SSC 1 of each of these sources vs. their $(V-I)_0$ colour. Cluster 11 is extremely red and off-scale in Fig. 10. Its extreme faintness in V may be due to localized increased dust absorption, or it may be a very red high-redshift background galaxy. Because of its peculiar colour, we shall not consider it further. The very blue colour of cluster 7 may be due to enhanced star-forming activity. Excluding source 11, we obtain 21.11 mag and 21.17 mag for the integrated apparent luminosity of the new sources in V and I respectively, corresponding in either band to $\lesssim 6\%$ of the luminosity of the LSB component. Fig. 10 shows a trend of increasing $(V-I)_0$ colour with increasing projected distance r from SSC 1, with a flattening beyond $r \sim 3\farcs5$. The reddening is probably due mainly to an aging of the stellar populations in the clusters (Thuan et al. 1997). The curves in Fig. 10 show the expected colour distribution with radius if we assume a self-propagating star formation scenario in which the star-forming activity in SBS 0335–052E started at the location of cluster 16 ~ 100 Myr ago and then propagated through the H I gas in the SE direction towards SSC 1 (age ~ 3 Myr) with a constant speed of ~ 18 km s^{-1}. Assuming that the properties of the ionized gas (dotted line) do not vary with time, the dashed line shows the evolutionary change of the $(V-I)$ colour when both the stellar and the observed gaseous emission play a role, while the solid line shows the colour behavior when there is only stellar emission. It is clear that the majority of the points are well fitted by the (gas + stars) dashed line. But a few clusters (6, 9, 12, 13, 15 and 16) are better fitted by the stellar line, implying that their colours are not contaminated by gaseous emission. The colour curves flatten out beyond a certain distance because, past ~ 10 - 20 Myr, $(V-I)$ changes very little with age. There is some scatter about the theoretical lines, which we attribute to varying dust absorption (Thuan et al. 1997). Izotov et al. (1997b) found that dust extinction with A_V up to 0.4 mag is present out to a distance of $\sim 4''$ to the NW of SSC 1. Therefore, the intrinsic $(V-I)$ colours of knots displayed in Fig. 10 can be bluer by

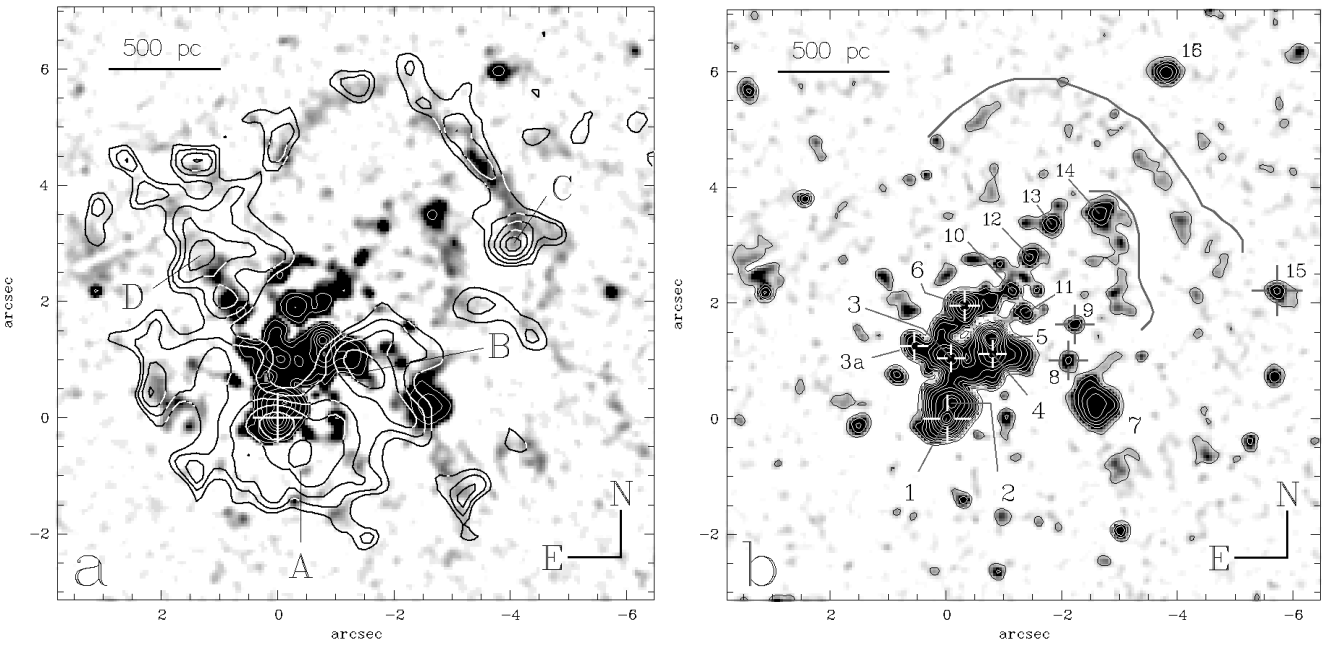

Fig. 9. **a** HST WFPC2 V image of SBS 0335–052E processed with a hierarchical binning technique. The overlayed contours correspond to extinction-corrected isochromes with $(V-I)_0$ varying from –0.7 to –0.3 mag in steps of 0.1 mag. The bluest regions with $(V-I)_0$ colours ranging between $\gtrsim$ –0.8 and –0.6 mag are indicated by A and B. Note that the bluest regions are offset relative to the positions of the brightest SSCs. The average $(V-I)_0$ colours for regions C and D at the tips of the supershell are respectively –0.7 and –0.6 mag. The $(V-I)_0$ of the supershell, at ∼1.4 kpc from SSC 1, ranges between –0.3 and –0.4 mag. **b** HST WFPC2 I image of SBS 0335–052E processed as the V-band image. Distinct star clusters roughly aligned along the galaxy's major axis are listed in Table 4. The positions of the supershell (at a distance of $\sim$ 1.4 kpc from SSC 1) and an inner shell (at $\sim$ 1 kpc and more clearly visible in the V-image) are delineated in the upper right by the thick lines.

∼0.2 mag than the observed values. The faint clusters to the NW of SSC 6 may be interpreted as the fossil remnants of a population of SSCs formed in the past which have dimmed by 2-3 mag within a time span of few Myr.

5.2. The age of the extended underlying stellar component in SBS 0335–052E

HST imaging in the V and I bands (Thuan et al. 1997) has revealed that the extended underlying component in SBS 0335–052E is very blue with $(V-I) \lesssim 0$. It becomes even bluer ($\sim -0.06 \pm 0.02$) if the compact sources superposed on the diffuse continuum are excluded (Sect. 4.1). Such a blue $(V-I)$ colour would be produced by a young stellar population not older than 10 Myr if the underlying emission is purely stellar in origin. The filamentary and patchy structure of the underlying component as well as its $(V-I)$ colour distribution (Fig. 9a) suggest that a significant fraction of its emission comes from ionized gas. This has been shown to be the case by the spectroscopic observations of Izotov et al. (1997b) who find strong emission lines as far as $\sim$ 2 kpc from SSC1. They found the equivalent width of the Hβ line to $\sim$ 3 times smaller than that expected for pure gaseous emission, i.e. the gaseous emission contributes $\sim$ 1/3 of the underlying emission while the stars contribute the remaining ∼2/3. The gaseous emission superposed on the stellar emission give bluer $(V-I)$ colours as compared to those from a pure stellar population. Since the $(V-I)$ colour of the extended underlying emission is $\sim$ 0.5 mag redder than the colour of the youngest clusters, the underlying stellar population is likely to be older than the SSCs.

In Table 5 we show the time evolution of the $(U-B)$, $(B-V)$, $(V-I)$, $(R-I)$ and $(V-K)$ colours of a stellar population made in a single instantaneous burst of star formation with a Salpeter IMF and upper and lower mass limits of 120 and 0.6 $M_\odot$ respectively, as it ages from 10 Myr to 10 Gyr. We used stellar parameters (effective temperature and luminosity) from isochrones with a heavy element mass fraction Z = 0.0004 calculated by Bertelli et al. (1994). The synthetic stellar SEDs have been computed using the stellar atmosphere library with metallicity $10^{-4} Z_\odot$ of Lejeune et al. (1997). The observed gaseous emission is then superposed on the calculated stellar emission, taking into account both the continuum and line contributions, and the resulting model is compared to the observed spectrum of the underlying component. To improve the signal-to-noise ratio of the latter, we have coadded one-dimensional spectra in the distance range 3″– 9″ (0.8 – 2.4 kpc) from the young stellar clusters. The spectrum of the underlying component is shown in Fig. 11 along with the total gaseous + stellar continuum of the best fit model which corresponds to an age of 50 Myr. Fig. 12 shows the contributions of the gaseous and stellar emissions separately. It is clear that there is an appreciable contribution from the ionized gas. The observed colours for the underlying

Table 4. Properties of stellar clusters in SBS 0335–052E

Clr.	Δ RA	Δ DEC	$(V-I)_0^{\alpha}$	V_0	I_0	r
	arcsec	arcsec	mag	mag	mag	arcsec
1	0.00	0.00	-0.61 ± 0.02	18.93 ± 0.10	19.54 ± 0.01	0.00
2	0.15	0.30	-0.39 ± 0.02	19.24 ± 0.02	19.63 ± 0.02	0.33
3	0.10	1.05	-0.26 ± 0.12	20.55 ± 0.08	20.81 ± 0.10	1.05
4	0.85	1.15	-0.15 ± 0.03	19.71 ± 0.02	19.86 ± 0.02	1.42
5	0.80	1.39	0.14 ± 0.04	19.50 ± 0.03	19.36 ± 0.03	1.61
6	0.35	1.99	0.31 ± 0.14	21.96 ± 0.11	21.65 ± 0.09	2.02
3a	–0.55	1.29	0.04 ± 0.12	23.60 ± 0.08	23.56 ± 0.09	1.41
7	2.59	0.25	-0.25 ± 0.08	21.58 ± 0.06	21.83 ± 0.06	2.60
8	2.14	1.00	-0.01 ± 0.18	25.56 ± 0.14	25.57 ± 0.11	2.36
9	2.24	1.64	0.27 ± 0.26	25.87 ± 0.14	25.60 ± 0.22	2.78
10	1.15	2.19	-0.21 ± 0.22	24.71 ± 0.10	24.92 ± 0.20	2.47
11	1.39	1.84	2.60 ± 0.52	27.35 ± 0.50	24.75 ± 0.15	2.31
12	1.44	2.79	0.42 ± 0.17	25.35 ± 0.14	24.92 ± 0.10	3.14
13	1.84	3.39	0.77 ± 0.18	25.43 ± 0.15	24.66 ± 0.10	3.86
14	2.64	3.54	-0.01 ± 0.15	24.01 ± 0.10	24.02 ± 0.11	4.41
15	5.73	2.19	0.55 ± 0.16	25.34 ± 0.13	24.79 ± 0.09	6.13
16	3.83	5.98	0.61 ± 0.15	24.26 ± 0.11	23.65 ± 0.10	7.10

$^{\alpha}$corrected for foreground extinction (A_V=0.1 mag, A_I=0.06 mag; Burstein & Heiles 1982). Photometric data for clusters 1 through 6 were taken from Thuan et al. (1997).

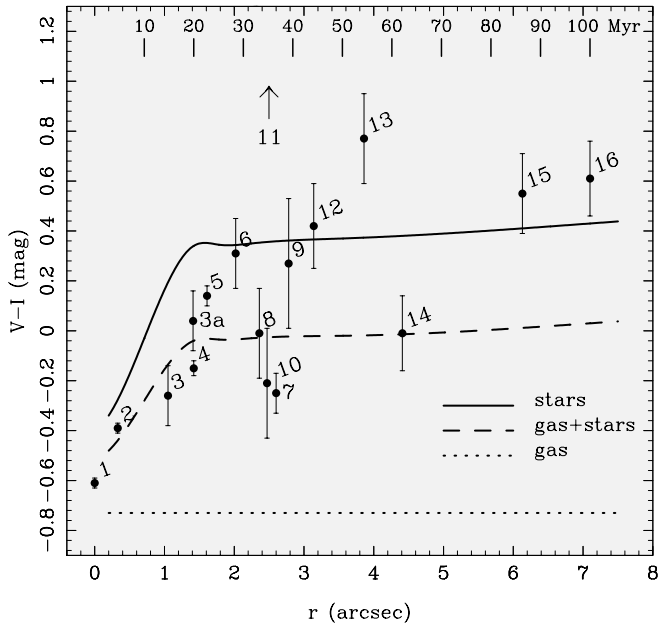

Fig. 10. Galactocentric distance vs. $(V-I)_0$ colour index for the compact regions identified along the major axis of SBS 0335–052E (Fig. 9b; Table 4). The very red ($(V-I) \sim 2.5$) source 11 is off-scale. The curves show the $(V-I)$ distribution expected to evolve if star formation was initiated ~ 100 Myrs ago near knot 16 and propagated with a constant speed of ~ 18 km sec^{-1} to its current location (SSC 1). The colour evolution for stellar, stellar+gaseous and gaseous emitting sources (Table 5) is shown by the solid, dashed and dotted curves, respectively.

component as derived from $UBVRI$ photometry are shown in the last row of Table 5. Inspection of Table 5 shows that, regardless of the age of the system, a pure stellar emission model

Table 5. Synthetic colours of the underlying component

log t	$U-B$	$B-V$	$V-I$	$R-I$	$V-K$
		a) Stellar emission			
7.0	–1.00	–0.15	–0.03	–0.08	–0.31
7.3	–0.83	–0.02	0.34	0.13	0.74
7.5	–0.72	0.01	0.35	0.13	0.73
7.7	–0.62	0.03	0.37	0.14	0.73
8.0	–0.49	0.07	0.43	0.17	0.83
8.1	–0.41	0.19	0.79	0.36	1.60
8.5	–0.25	0.23	0.83	0.38	1.66
8.9	–0.20	0.38	0.96	0.42	1.82
9.5	–0.13	0.50	0.96	0.41	1.80
10.0	–0.23	0.65	1.14	0.48	2.06
		b) Stellar and gaseous emission			
7.0	–0.88	0.16	–0.28	–0.41	0.42
7.3	–0.77	0.23	–0.04	–0.26	0.75
7.5	–0.69	0.25	–0.03	–0.25	0.75
7.7	–0.62	0.26	–0.02	–0.24	0.75
8.0	–0.55	0.28	0.03	–0.21	0.80
8.1	–0.51	0.34	0.31	–0.02	1.27
8.5	–0.44	0.37	0.34	0.00	1.31
8.9	–0.42	0.44	0.47	0.07	1.44
9.5	–0.42	0.51	0.49	0.07	1.44
10.0	–0.47	0.59	0.66	0.17	1.68
obs	–0.7	0.25÷0.30	0.0	–0.3	...

fails to reproduce the observed colours of this underlying component. By contrast, a model including both stellar and gaseous emission can account for the observed colours fairly well. The ages derived for the stellar population are in the range between 20 and 100 Myr, with the best fit corresponding to an age of 30 Myr. As discussed in Sect. 5.2, the $(U-B)$ colour shows little

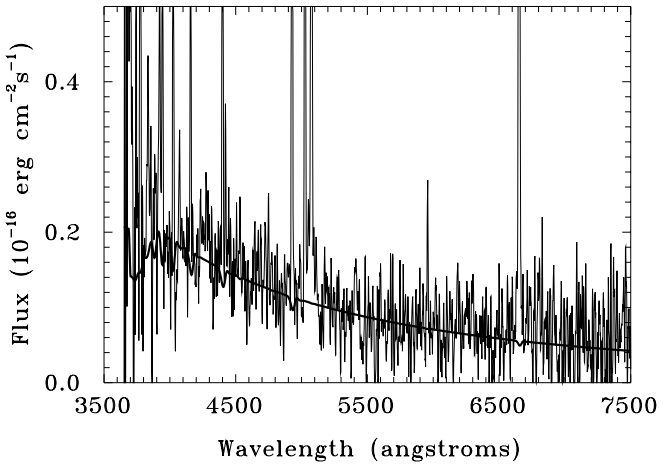

Fig. 11. Spectrum of the underlying component of SBS 0335–052E (thin line) on which is superposed the sum of the SEDs of the model stellar population with age 50 Myr and of the observed gaseous continuum (thick line).

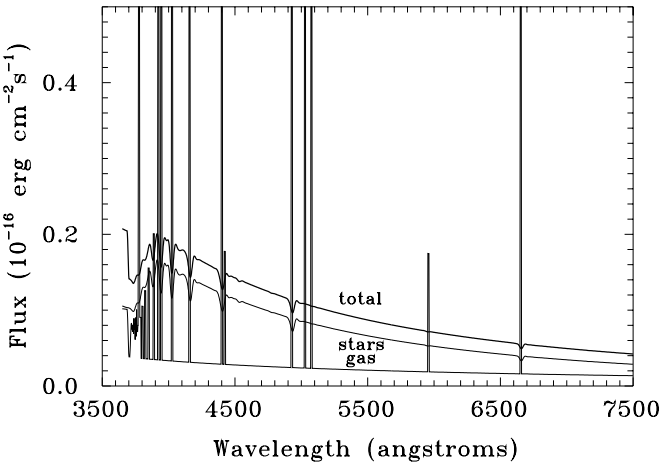

Fig. 12. The respective contributions of gaseous and stellar emission in the extended underlying LSB component of SBS 0335–052E (thin lines). The composite continuum spectral energy distribution is shown by the thick line.

sensitivity to the contribution of gaseous emission. This is also the case for the $(V-K)$ colour at ages between 10 and 100 Myr. On the other hand, the $(V-I)$ colour is most sensitive to gaseous emission, providing thereby an essential constraint in disentangling the relative contributions of stellar and gaseous emission. Population synthesis models allow us to put a firm upper limit of $\lesssim 100$ Myr for the age of the underlying stellar component (Table 5). AGB stars are present in models with age greater than 100 Myr, which make the $(V-I)$ colour jump by $\sim$0.3 mag, and become too red to be consistent with the observed value.

Integrating the B SBP of SBS 0335–052E (Fig. 2) gives apparent magnitudes of 17.4 and 18.2 mag, and absolute magnitudes of –16.3 and –15.5 mag respectively for the starburst and LSB components. Thus, the starburst component is twice as luminous as the LSB component.

Adopting an absolute B magnitude of –0.9 mag for a stellar cluster with age 3 Myr and mass normalized to 1 $M_\odot$, a Salpeter IMF and lower and upper mass limits of 0.8 and 120 $M_\odot$ (Schaerer & Vacca 1998), we obtain a total stellar mass in the starburst of 1.4×10^6 $M_\odot$. Population synthesis models predict that, for equal initial masses, the B luminosity of an older underlying stellar population with age 100 Myr is ~ 2.5 times lower than the B luminosity at an age of 3 Myrs. Since the B luminosity of the extended underlying component is ~ 2 times lower than that of the starburst, this would imply that the stellar mass in the LSB component of SBS 0335–052E is ~ 1.2 times larger than the stellar mass in the starburst component. Hence, the mass of the underlying component is 1.7×10^6 $M_\odot$ and the total stellar mass of SBS 0335–052E is about 3.1×10^6 $M_\odot$, $\sim$3 times smaller than that inferred by Thuan et al. (1997). Note, however, that the extension of a Salpeter IMF to a low mass limit from 0.8 $M_\odot$ to 0.1 $M_\odot$ (the value used by Thuan et al. 1997) would result in a $\sim$12 times larger stellar mass. The mass of the neutral gas in SBS 0335–052 is about 2×10^9 $M_\odot$ and its dynamical mass is $\sim 8\times10^9$ $M_\odot$ (Pustilnik et al. 1998). Therefore, the stellar-to-H I mass in SBS 0335–052E is $\sim 0.15\%$ and the mass-to-light ratio for SBS 0335–052 E+W ~ 10. In summary, SBS 0335–052E is a dwarf galaxy in its infancy, making its first stars less than 100 Myr ago and with the bulk of its total mass still in the form of primordial H I gas unpolluted by stellar metal enrichment (Thuan & Izotov 1997).

Notwithstanding the difference in absolute magnitudes and star formation rates of SBS 0335–052E and high-redshift star-forming galaxies, they seem to share several physical and morphological properties. Bunker et al. (1997) and Frye & Broadhurst (1998) have studied the properties of a possibly primeval galaxy at a redshift z = 4.04 and derived a relatively high intrinsic column density N(H I) = 3×10^{21} cm^{-2} from damped Ly-α absorption spectroscopy. This value compares well with N(H I) = 7×10^{21} cm^{-2} derived by Thuan & Izotov (1997) for SBS 0335–052E. Franx et al. (1997) have studied an even more distant galaxy at a redshift z = 4.92, one of the highest redshift objects known. They found that the galaxy has an asymmetric structure, containing a bright knot with effective radius of $130h_{50}^{-1}$ pc and a patch of extended emission with a $\sim$10 times larger radius. This extended patch is partially resolved into compact star-forming regions and could be formed through propagating star formation processes. Thus, SBS 0335–052E being one of the best examples of a nearby young dwarf galaxy may be viewed as a convenient laboratory for studying physical processes occuring at the early epoch of galaxy formation.

5.3. A 10 Gyr old stellar population?

Although the evidence is compelling that most of the stellar emission in the LSB component of SBS 0335–052E is from a stellar population with age $\lesssim 100$ Myrs, we cannot definitely rule out the presence of very old stars with age ~ 10 Gyr, since such a population would cause a barely detectable colour effect.

Table 6. Colours of a composite mixture of young (100 Myr), old (10 Gyr) stellar populations and gaseous emission

Relative mass of the old population	$U-B$	$B-V$	$V-I$	$R-I$	$V-K$
0.00	–0.61	0.28	0.01	–0.23	0.79
0.50	–0.61	0.29	0.03	–0.22	0.83
0.90	–0.61	0.34	0.16	–0.13	1.04
0.95	–0.60	0.39	0.26	–0.08	1.18
0.99	–0.59	0.50	0.45	0.04	1.45
1.00	–0.59	0.57	0.55	0.10	1.58

In Table 6 we show the colours for a composite mixture of a young (100 Myr) stellar population, an old (10 Gyr) one and ionized gas, the emission of which is derived from the observed emission line fluxes and equivalent widths. The mean observed $(V-I)$ colour of the underlying component of SBS 0335–052E in the region from $4''$ to $6''$ is $\lesssim 0$ mag. Given the significant photometric uncertainties ($\pm$0.2 in $(V-I)$) at these large distances from the young clusters (Fig. 5), we cannot dismiss the possibility of the presence of an old stellar population with mass as much as ~ 10 times the mass of the young stellar population (corresponding to a relative mass fraction of 0.9 of the old stellar population in Table 6). We do not believe, however, the existence of such an old stellar population to be plausible, because of the following reasons. First, if an old stellar population of mass $\sim 10^8$ $M_\odot$ was formed in a burst 10 Gyr ago, it is difficult to understand why a second burst of star formation did not occur until $\sim$100 Myr. Probably the input of energy resulting from supernovae in the first burst could not have prevented further star formation for a whole Hubble time. Second, a previous burst of star formation would have produced oxygen in excess of the value 12+log(O/H) = 7.30 observed in the star-forming region (Melnick et al. 1992; Izotov et al. 1997b). Melnick et al. (1992) measured a $L(\mathrm{H}\beta)\sim 1.8\times10^{40}$ erg s^{-1} which gives an equivalent number of $\sim$ 4500 O7 stars in the present burst (Thuan et al. 1997). These stars can synthesize $\sim 9\times10^3$ $M_\odot$ of oxygen if we assume that ~ 2 $M_\odot$ of oxygen is produced by a single zero-metallicity star with mass 25 $M_\odot$ (Woosley & Weaver 1995). Adopting a mean electron number density of $\sim$10 cm^{-3} , the total mass of the H II region is $\sim 3\times10^7$ $M_\odot$. The total amount of oxygen synthesized by the massive stars in the present burst would result in an oxygen abundance of 12+log(O/H) $\sim$ 7.4, assuming uniform mixing. This is very close to the observed value. Thus, the massive stars in the present burst are sufficient for producing the observed oxygen abundance. An old stellar population with mass ~ 10 times larger than that of the young population would produce a 10 times higher oxygen abundance, assuming that the metals have not been driven out into the neutral gas or into the intergalactic medium via galactic winds. That this is not the case has been suggested by Thuan & Izotov (1997) who argued that the H I envelope of SBS 0335–052 is devoid of any metal enrichment.

In summary, there is no need to postulate any stellar population older than ~ 100 Myr to account for the spectrophotometric properties of SBS 0335–052E. If, however, an old stellar component is present, then its mass cannot exceed the mass of the young stellar population without overproducing the metals. A definitive check of such a possibility requires deep near-infrared photometric observations.

5.4. The properties of SBS 0335–052W

The fainter western component of SBS 0335–052 is also characterized by very blue $(U-B)$ and $(R-I)$ integrated colours, only slightly redder than those inferred for SBS 0335–052E (Table 1). The morphology and integrated colours of SBS 0335–052W show that it contains at least two star-forming regions and suggest that it is also young. The spectrum of SBS 0335–052W is that of a low-metallicity high-excitation supergiant H II region with strong emission lines. Lipovetsky et al. (1998) have derived an oxygen abundance 12+log(O/H) $\sim$ 7.13–7.22, even lower than the value obtained for SBS 0335–052E. However, the intensities and equivalent widths of Hβ and other strong emission lines in SBS 0335–052W are smaller than in the spectrum of SBS 0335–052E, suggesting a slightly larger age of the ionizing young stellar clusters. Ground-based surface photometry shows the $(U-B)$ colour to vary between ~ -0.7 mag and ~ -0.2 mag. However, the large uncertainties caused by the compactness and faintness of SBS 0335–052W do not allow an analysis of its evolutionary status.

6. Summary and conclusions

HST observations (Thuan et al. 1997) and MMT spectroscopy (Izotov et al. 1997b) of the BCD SBS 0335–052 (Izotov et al. 1990) are combined with ground-based U and B photometry to constrain its evolutionary status.

The U, B, V and I surface brightness profiles (SBPs) of SBS 0335–052E all show an exponential intensity decrease for radii $\gtrsim 4''$ with a luminosity excess above the outer exponential fit in the inner parts. The radially averaged $(U-B)$ and $(V-I)$ colour profiles for the LSB underlying component of SBS 0335–052E show nearly constant colours, -0.75 ± 0.1 mag and -0.06 ± 0.02 mag, respectively. Spatially resolved HST $(V-I)$ colour maps show, however, the two-dimensional colour distribution in SBS 0335–052E to be inhomogeneous, with extended regions having $(V-I)$ colours as blue as $\lesssim -0.7$ mag. The bluest regions are typically shifted by $\sim 1''$ (~ 260 pc) with respect to the position of the brightest SSCs. This shift implies that emission by ionized gas dominates the light of SBS 0335–052E on scales of several 100 pc, corroborating the spectroscopic evidence of Izotov et al. (1997b). The derived structural properties of the LSB underlying component of SBS 0335–052E are similar to those of other BCDs (Papaderos et al. 1996b).

Emission from ionized gas contributes significantly ($\sim$ 30%; Izotov et al. 1997b) to the light of the LSB component. Thus, a derivation of the intrinsic colours of the stellar population in the underlying component of SBS 0335–052E requires a

correction for gaseous contamination. We found that the spectrophotometric properties of the LSB underlying component in SBS 0335–052E can be accounted for by a stellar population of mass $\sim 3 \times 10^6$ $M_\odot$ and not older than ~ 100 Myr. A stellar population older than that age would produce too red $(V-I)$ colours because of the appearance of asymptotic giant branch stars. The possibility of an underlying old (10 Gyr) stellar population with ~ 10 times greater mass cannot be definitely ruled out, since such a population would cause a barely detectable colour change. We consider, however, this possibility to be unlikely because metals would be overproduced in the event of a previous burst. These metals would not have escaped into the H I envelope surrounding the BCD as Thuan & Izotov (1997) have argued that the H I gas has an extremely low metallicity and can even be primordial.

Using V and I HST images, Thuan et al. (1997) have shown that most of the current star formation activity occurs within 6 SSCs roughly aligned in the NW-SE direction. The $(V-I)$ colours of these SSCs show a systematic reddening away from the brightest SSC, which Thuan et al. (1997) attributed mainly to an aging effect due to self-propagating star formation in the BCD. We have reprocessed the HST data of Thuan et al. (1997) with a technique better suited for identifying faint sources, to an intensity level comparable to that of the diffuse underlying LSB component. We were able to detect and photometrically study several fainter compact objects lying further along the NW-SE direction. We found the reddening trend reported by Thuan et al. (1997) to continue out to $\sim 7''$ (~ 1.8 kpc) from the brightest and youngest SSC 1, thus strengthening the propagating star formation picture. Assuming that star formation started ~ 100 Myrs ago in the source which is reddest and furthest away (at ~ 1.8 kpc) from SSC 1 (age ~ 3 Myr), we derive an average speed of $\lesssim 20$ km s^{-1} for the propagation of star formation, comparable to the average sound speed within the H I gas.

The dwarf galaxy SBS 0335–052W, resides within the same H I complex roughly 22 kpc westwards of SBS 0335–052E, at the location of the other peak in H I column density in the H I VLA map by Pustilnik et al. (1998). The western dwarf consists of at least two star-forming regions embedded within a LSB component with an exponential intensity profile and a B central surface brightness ~ 1 mag fainter than SBS 0335–052E. Its very blue integrated $(U-B)$ colour index (-0.54 ± 0.1 mag) along with its very low metallicity ($Z_\odot/40$) suggest that it is not much older than its eastern counterpart.

Acknowledgements. We are grateful to K. Bischoff and W. Pietsch who kindly obtained for us the U and B images at La Silla. Y.I.I. and N.G.G. thank the Universitäts–Sternwarte of Göttingen for warm hospitality. Y.I.I. thanks D. Schaerer for the stellar evolutionary synthesis models prior to their publication. Research by P.P. and K.J.F. has been supported by Deutsche Agentur für Raumfahrtangelegenheiten (DARA) GmbH grant 50 OR 9407 6. K.J.F, P.P., Y.I.I and N.G. acknowledge the support of Volkswagen Foundation Grant No. I/72919. T.X.T. and Y.I.I. have been supported partially by NATO collaborative research grant 921285 and NSF grant AST-9616863.

References

Aller L. H., 1984, Physics of Thermal Gaseous Nebulae. Dordrecht: Reidel
Bertelli G., Bressan A., Chiosi C., Fagotto F., Nasi E., 1994, A&AS 106, 275
Bunker A., Moustakas L., Davis M., Frye B., Broadhurst T., Spinrad H. 1997, astro-ph/9712173
Burstein D., Heiles C., 1982, AJ 87, 1165
Ferland G. J., 1980, PASP 92, 596
Franx M., Illingworth G. D., Kelson D., VanDokkum P. G., Pieter G., Tran K., 1997, ApJ 486, L75
Frye B., Broadhurst T., 1998, ApJ 499, L115
Giavalisco M., Koratkar A., Calzetti D., 1996, ApJ 461, 831
Izotov Y. I., Lipovetsky V. A., Guseva N. G., Kniazev A. Y., Stepanian J. A., 1990, Nature 343, 238
Izotov Y. I., Thuan T. X., Lipovetsky V. A., 1994, ApJ 435, 647
Izotov Y. I., Thuan T. X., Lipovetsky V. A., 1997a, ApJS 108, 1
Izotov Y. I., Lipovetsky V. A., Chaffee F. H., Foltz C. B., Guseva N. G., Kniazev A. Y., 1997b, ApJ 476, 698
Kunth D., Maurogordato S., Vigroux L., 1988, A&A 204, 10
Landolt A. U., 1992, AJ 104, 340
Lejeune T., Cuisinier F., Buser R., 1997, A&AS 125, 229
Lipovetsky V. A., Chaffee F. H., Izotov Y. I., Foltz C. B., Kniazev A. Y., Hopp U., 1998, ApJ submitted
Loose H.-H., Thuan T. X., 1985. In D. Kunth, T. X. Thuan, J. Tran Van (eds.). Star-Forming Dwarf Galaxies. Gif-sur-Yvette: Edition Frontières, p. 73
Melnick J., Heydari-Malayeri M., Leisy P., 1992, A&A 253, 16
O'Connell R.W., Gallagher J.S., Hunter D.A., 1994, ApJ 433, 65
Papaderos P., Loose H.-H., Thuan T. X., Fricke K. J., 1996a, A&AS 120, 207
Papaderos P., Loose H.-H., Fricke K.J., Thuan T. X., 1996b, A&A 314, 59
Papaderos P., Fricke K.J., Thuan T.X., 1998, in preparation
Pustilnik S. A., Lipovetsky V. A., Izotov Y. I., Brinks E., Thuan T. X., Kniazev A. Y., Neizvestny S. I., Ugryumov A. V., 1997, Pis'ma v A.Zh. 23, 350
Pustilnik S. A., Thuan T. X., Brinks E., Lipovetsky V. A., Izotov Y. I., 1998, in preparation
Sargent W. L. W., Searle L., 1970, ApJ 162, L155
Schaerer D., Vacca W. D., 1998, ApJ 497, 618
Searle L., Sargent W. L. W., 1972, ApJ 173, 25
Steidel C. C., Giavalisco M., Pettini M., Dickinson M., Adelberger K. L., 1996, ApJ 462, L17
Telles E., Terlevich R., 1997, MNRAS 286, 183
Thuan T. X., Martin G. E., 1981, ApJ 247, 823
Thuan T.X., 1991, in Massive Stars in Starbursts, eds. C. Leitherer, N.R. Walborn, T.M. Heckman, C.A. Norman, Cambridge University Press, p. 183
Thuan T. X., Izotov Y. I., Lipovetsky V. A., 1996, ApJ 463, 120
Thuan T. X., Izotov Y. I., 1997, ApJ 489, 623
Thuan T. X., Izotov Y. I., Lipovetsky V. A., 1997, ApJ 477, 661
Woosley S. E., Weaver T. A., 1995, ApJS 101, 181